ACS APPLIED MATERIALS & INTERFACES

Research Article

www.acsami.org

Rattle-type Carbon–Alumina Core–Shell Spheres: Synthesis and Application for Adsorption of Organic Dyes

Jiabin Zhou,[†] Chuan Tang,[†] Bei Cheng,[†] Jiaguo Yu,*[,†] and Mietek Jaroniec*[,‡]

[†]State Key Laboratory of Advanced Technology for Materials Synthesis and Processing and School of Resources and Environmental Engineering, Wuhan University of Technology, Wuhan 430070, P. R. China

[‡]Department of Chemistry & Biochemistry, Kent State University, Kent, Ohio 44242, United States

Supporting Information

ABSTRACT: Porous micro- and nanostructured materials with desired morphologies and tunable pore sizes are of great interests because of their potential applications in environmental remediation. In this study, novel rattle-type carbon–alumina core–shell spheres were prepared by using glucose and metal salt as precursors via a simple one-pot hydrothermal synthesis followed by calcination. The microstructure, morphology, and chemical composition of the resulting materials were characterized by X-ray diffraction (XRD), energy dispersive X-ray spectroscopy (EDX), scanning electron microscopy (SEM), transmission electron microscopy (TEM), and N_2 adsorption–desorption techniques. These rattle-type spheres are composed of a porous Al_2O_3 shell (thickness ≈ 80 nm) and a solid carbon core (diameter ≈ 200 nm) with variable space between the core and shell. Furthermore, adsorption experiments indicate that the resulting carbon–alumina particles are powerful adsorbents for the removal of Orange-II dye from water with maximum adsorption capacity of ~210 mg/g. It is envisioned that these rattle-type composite particles with high surface area and large cavities are of particular interest for adsorption of pollutants, separation, and water purification.

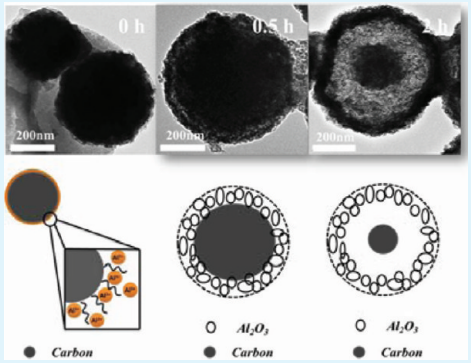

KEYWORDS: *rattle-type spheres, carbon-alumina, hollow spheres, adsorption, organic dyes*

1. INTRODUCTION

In recent years, the fabrication of inorganic micro- and nanosized hollow and rattle-type core/shell materials has attracted a lot of attention because of the materials' versatile applications including catalysts, chemical sensors, medicine, drug/gene reservoirs, and adsorbents.[1−5] These core–shell composites often exhibit relatively high surface area, increased stability and superior magnetic and optical properties.[6,7] The major strategies to prepare such structures are based on the use of various templates including hard and soft templates, as well as template-free routes.[8−15] Recently, the colloidal carbonaceous spheres have been employed as a green and novel template to synthesize hollow structures of a variety of materials.[16−18] The resulting products inherit the spherical morphology of the carbon particles and possess favorable porous properties.

Nowadays the rattle-type nanoarchitectures, a special class of core/shell particles, have been extensively studied because of their unique structural properties and potential applications. These architectures possess spherical shells and solid cores having a variable space between them.[19] Some rattle-type particles such as Au-polymer, SiO_2–Fe_2O_3 nanoball, and Cu-silica have been synthesized;[20−22] however, the existing synthesis strategies are often complicated because of tedious procedures and poor reproducibility. Thus, there is still a challenge to develop simple, controllable, and environmentally friendly methods for the synthesis of the rattle-type particles.

Herein, we present a facile and effective strategy to fabricate rattle-type carbon–alumina core–shell spheres with large cavities using colloidal carbon spheres as hard templates. The as-prepared products exhibit spherical morphology, relatively high surface area, and porous structures. Experimental study of their performance as adsorbents for dye pollutants from water showed that they are very promising materials for wastewater treatment.

2. EXPERIMENTAL SECTION

Sample Preparation. All the chemicals were analytical grade from Shanghai Chemical Industrial Company and were used without further purification. In a typical synthesis, 20.1 mmol of glucose and the desired amount of aluminum nitrate (2.01, 4.02, 10.05 mmol) were respectively dissolved in 60 mL of distilled water under vigorous stirring. When the mixture solution was fully dissolved, 10 mL of ethanol were added under stirring. The resultant mixture was placed in a 100 mL Teflon-lined stainless steel autoclave and heated at 180 °C for 24 h. The black products were then collected, washed three times with water and ethanol, and dried at 80 °C for 5 h. To obtain the rattle-type carbon–alumina spheres, we heated the dried products at

Received: January 31, 2012
Accepted: March 29, 2012
Published: March 29, 2012

   dx.doi.org/10.1021/am300176k | ACS Appl. Mater. Interfaces 2012, 4, 2174–2179

450 °C for 2 h. Because the molar ratio of glucose and aluminum nitrate varied from 2, 5, to 10, the carbon−alumina samples were denoted as CAl-2, CAl-5, and CAl-10, respectively. The detailed synthesis conditions and physical properties of the samples are shown in Table 1. For the purpose of comparison, commercial alumina sample (Al_2O_3) was examined too.

Table 1. Physical Properties of the Samples Studied

sample	average pore size (nm)	pore volume (cm^3/g)	BET surface area (m^2/g)
CAl-2	5.8	0.15	105
CAl-5	4.9	0.19	160
CAl-10	4.5	0.21	182
Al_2O_3	4.4	0.01	9

Characterization. Powder X-ray diffraction (XRD) patterns of the as-prepared samples were obtained on an X-ray diffractometer (type HZG41B-PC) using Cu K_α radiation at a scan rate of 0.05° 2θ s^{-1}. The morphology of all samples was observed on an S-4800 field emission scanning electron microscopy (FE-SEM, Hitachi, Japan) at an accelerating voltage of 10 kV and linked with an Oxford Instruments X-ray analysis system. Transmission electron microscopy (TEM) analyses were conducted on a JEM-2100F electron microscope (JEOL, Japan) using a 200 kV accelerating voltage. The Brunauer−Emmett−Teller (BET) surface area of the powders was analyzed by nitrogen adsorption on a Micromeritics ASAP 2020 nitrogen adsorption apparatus (U.S.A.). All the samples were degassed at 150 °C prior to nitrogen adsorption measurements. The BET surface area was determined by a multipoint BET method using the adsorption data in the relative pressure (P/P_0) range of 0.05−0.3. Adsorption branches of the isotherms were used to determine the pore-size distributions for the samples studied via the Barrett−Joyner−Halenda (BJH) method, assuming a cylindrical pore model.[23] The volume of nitrogen adsorbed at the relative pressure (P/P_0) of 0.994 was used to determine the pore volume.

Batch Equilibrium and Kinetic Studies. Adsorption isotherm experiments were performed by adding a specified amount of the adsorbent samples (5 mg) to a series of beakers containing 25 mL of diluted Orange-II (O−II) solutions (15−50 mg/L). The pH value of the solution was maintained at 5−6 by adding 0.1 M NaOH or 0.1 M HCl solutions. The beakers were sealed and kept at air-bath oscillator under 25 °C for 24 h to reach equilibrium. The beakers were then removed from the oscillator, and the final concentration of O−II in the solution was measured at the maximum absorption wavelength of O−II (485 nm) using UV/vis spectrophotometer (Shimadzu UV/vis 2550 Spectrophotometer, Japan). The amount of O−II adsorbed at equilibrium q_e (mg/g) was calculated using the following equation:

$$q_e = \frac{(C_0 - C_e)V}{W} \quad (1)$$

where C_0 and C_e (mg/L) are the liquid phase initial and equilibrium concentrations of O−II, respectively, V is the volume of the solution (L), and W is the mass of adsorbent used (g).

The adsorption kinetic experiments were basically identical as those involving adsorption isotherm measurements. Adsorption kinetics of O−II was studied at three temperatures (25, 35, and 45 °C) in an air-bath oscillator. In a typical experiment, the initial concentration of the solution is fixed as 25 mg/L. The aqueous samples were taken at preset time intervals and the concentrations of O−II were similarly measured. The amount adsorbed at time t, q_t (mg/g), was calculated by:

$$q_t = \frac{(C_0 - C_t)V}{W} \quad (2)$$

where C_0 and C_t (mg/L) are the liquid phase concentrations of O−II at initial and specified time t, respectively, V is the volume of the solution (L), and W is the mass of adsorbent used (g).

3. RESULTS AND DISCUSSION

XRD Studies. The phase structure and relative crystallinity of the as-prepared samples were investigated by XRD. As can be seen from Figure 1, the main diffraction peaks for CAl-2 in

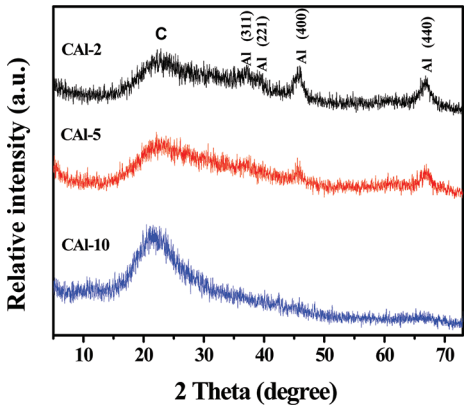

Figure 1. XRD patterns of the CAl-2, CAl-5 ,and CAl-10 samples (C represents the carbon sphere, whereas Al refers to γ-Al_2O_3).

the 2θ range from 30 to 70° can be easily assigned to cubic γ-Al_2O_3 (JCPDS 10−0425) with lattice parameters a = 7.90, b = 7.90, c = 7.90 Å. The broad and weak peaks of Al_2O_3 suggest its poor cystallinity and high water content.[24] The intensity of γ-alumina peaks decreases with increasing amount of carbon in the composite; they are almost invisible in the case of CAl-10. These very weak diffraction peaks for CAl-10 suggest that the high amount of glucose probably inhibits the crystallization of Al_2O_3. The broad peak in the 2θ region of 17−30° refers to amorphous carbon; its intensity increases with increasing amount of carbon in the composite.

Morphology. SEM and TEM were used to further investigate the morphology and microstructure of the samples. Images a and b in Figure 2 show the SEM images of the carbon spheres obtained by using only glucose as a carbon precursor at 180 °C for 8 h; fine monodispersed spheres with average

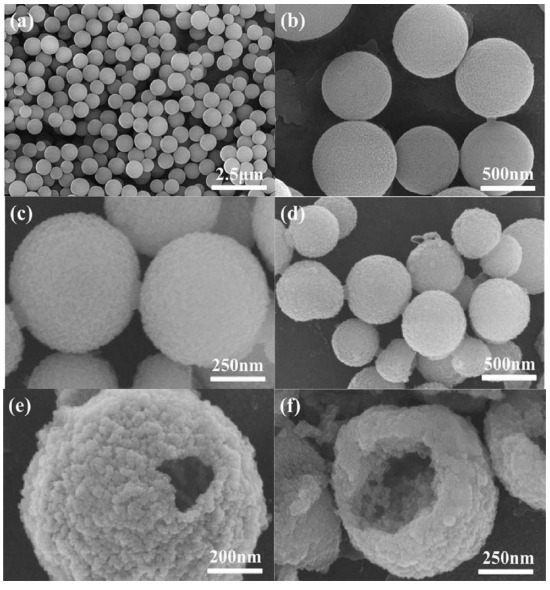

Figure 2. SEM images of (a , b) carbon spheres and (c−f) CAl-5 sample.

dx.doi.org/10.1021/am300176k | ACS Appl. Mater. Interfaces 2012, 4, 2174−2179

diameter of 650 nm are clearly visible. As shown in images c and d in Figure 2, the as-prepared carbon–alumina samples exhibit regular spherical shape with coarse surface, implying that the resulting particles inherited the spherical morphology from the solid carbon spheres (see Figure 3a, b). The carbon–

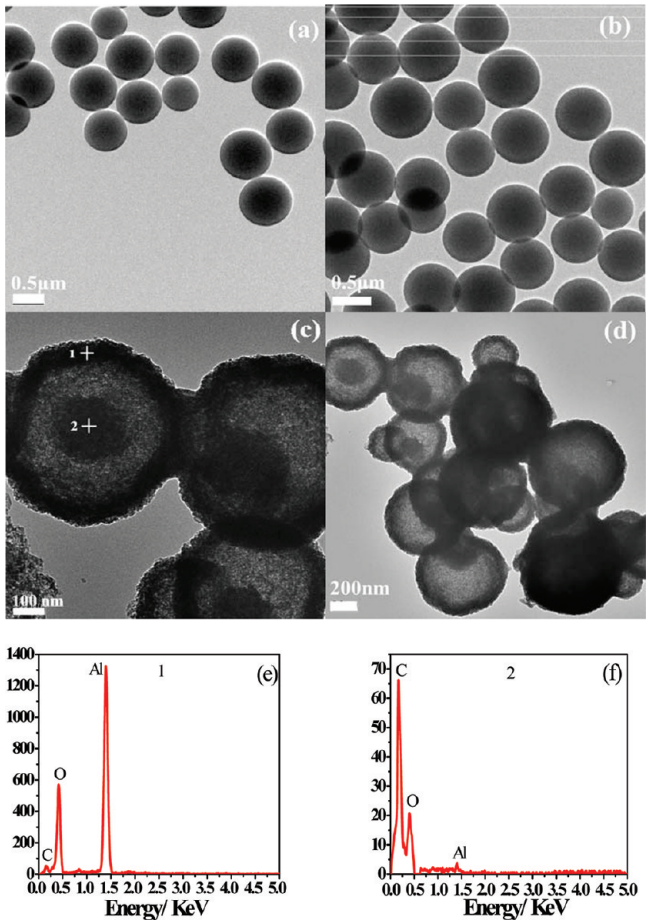

Figure 3. TEM images of (a, b) carbon spheres and (c, d) CAl-5; (e, f) selected area EDX patterns of the CAl-5 sample.

alumina spheres possess diameters of about 450–500 nm, which are smaller than those of glucose-based carbon particles due to the contraction upon thermal treatment. The broken spheres (Figure 2e, f) imply a hollow geometry of the final particles. Moreover, the TEM images of the samples (Figure 3c, d) further confirm the hollow structure of composite particles, which can be defined as rattle-type carbon–alumina spheres. Within a typical sphere, the thickness of Al_2O_3 shell is nearly 80 nm, while the diameter of the carbon core is about 200 nm with variable space between the core and shell. Meanwhile, the corresponding EDX pattern of an individual shell (area 1; see Figure 3e) reveals that the shell is mainly composed of Al_2O_3. Further EDX analysis (Figure 3f) of the core (area 2) shows that its major elemental composition is carbon. Therefore, it can be inferred from the above results that the as-prepared samples can be considered as the well-organized carbon–alumina spherical superstructures.

Surface Area and Porosity. Nitrogen adsorption–desorption isotherms and the corresponding pore size distribution curves for the samples studied are shown in Figure 4, respectively. The shape of all isotherms is type IV (Brunauer-Deming-Deming-Teller classification), which is characteristic of

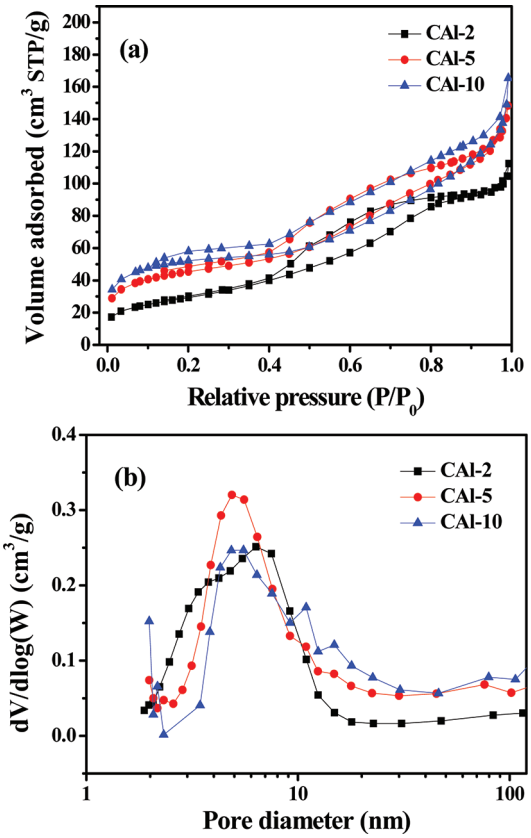

Figure 4. (a) Nitrogen adsorption–desorption isotherms and (b) the corresponding pore size distribution curves of the CAl-2, CAl-5, and CAl-10 samples.

mesoporous materials (2–50 nm). As can be seen from Figure 4, each isotherm has a typical hysteresis loop in the range of 0.4–0.8 P/P_0, indicating the presence of mesopores (having widths of about 5–7 nm). The hysteresis loops of the samples studied close at the limiting pressure; they are formed by gradually increasing/decreasing adsorption/desorption branches, respectively, indicating possible pore constrictions. Moreover, the observed increase in the hysteresis loops at relative pressures approaching 1.0 suggests the presence of larger mesopores and/or macropores. The pore structure parameters of the samples studied, such as the specific surface area, pore size and pore volume, are listed in Table 1. The surface area and pore volume of the carbon–alumina samples increase with increasing the C/Al^{3+} molar ratio. It is noteworthy that the specific surface area of the sample CAl-10 is approximately 20 times larger than that of Al_2O_3, which would be beneficial for the fast adsorption and transfer of adsorbate inside the hierarchically porous structure of this sample.

Formation Mechanism. The formation mechanism of the rattle-type carbon–alumina particles can be envisioned as a two-step process. First, the carbohydrate used as a carbon precursor is subjected to dehydration, condensation, polymerization and aromatization,[25] and finally carbon spheres are formed. The surface of these carbon spheres is hydrophilic because it contains a considerable amount of reactive oxygen-containing groups.[26] Therefore, Al^{3+} ions are easily attached to the surface of the aforementioned carbon spheres.[27] During this hydrothermal process, the Al^{3+} ions catalyze the formation of carbon spheres by accelerating hydrothermal reactions and

dx.doi.org/10.1021/am300176k | ACS Appl. Mater. Interfaces 2012, 4, 2174–2179

facilitating carbonization of the carbohydrate in aqueous solution. Also, these ions are precursors for the formation of alumina shells.

The subsequent calcination treatment is the key step in the formation of the rattle-type particles. According to the previous TGA studies,[28,29] the carbonaceous material shows a very low mass loss in the initial heating period, during which only water and other evaporable components are removed. This material begins to react with oxygen at about 330 °C and achieves its highest extent of decomposition at about 450 °C.[29]

The time-dependent evolution of morphology was elucidated by TEM and it is shown in Figure 5. The alumina−carbon

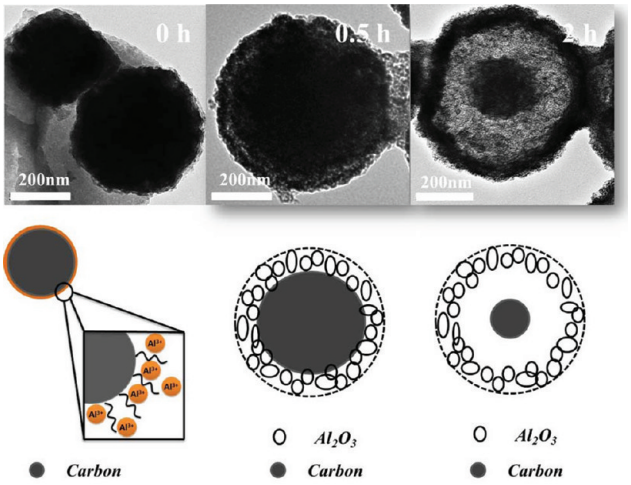

Figure 5. Schematic illustration of the formation of rattle-type carbon−alumina particles; TEM images represent the samples obtained by calcination at 450 °C for 0, 0.5, and 2 h, respectively.

composite microspheres were obtained via hydrothermal treatment before calcination. After calcination at 450 °C for 0.5 h, the carbon transforms into carbon dioxide, meanwhile the loosely adsorbed Al^{3+} ions turn into dense Al_2O_3 network forming the shells of the rattle-type spheres.[30] A closer observation of the TEM images reveals that there are small cavities between the carbon cores and alumina shells resulting from the shrinkage during calcination process. The 2 h calcination results in the partial removal of carbon cores, and simultaneous densification and cross-linking of the incorporated aluminum ions in the shells, which leads to the formation of rattle-type structures.

Adsorption Kinetics. Because of the unique hollow structure and high BET specific surface area, the rattle-type composite particles may possess high adsorption capacity toward various pollutants in water. Thus, the adsorption performance of the carbon−alumina particles for the removal of organic pollutants from water was investigated by the batch-type adsorption kinetic experiments.[31] In the present study, Orange-II ($C_{16}H_{11}N_2NaO_4S$), an anionic dye, was chosen as the model pollutant in water. Figure 6 shows the adsorption kinetics of O−II on the carbon−alumina samples and a commercial Al_2O_3 sample obtained by batch-type kinetic experiments at an initial O−II concentration of 25 mg/L at pH 5.0−6.0. The adsorption amount of O−II on the carbon−alumina samples increased rapidly within the initial 100 min and then became gradually constant, whereas the commercial Al_2O_3 sample exhibited a very low adsorption rate all the time. As shown in Figure 6, adsorption equilibrium can be reached

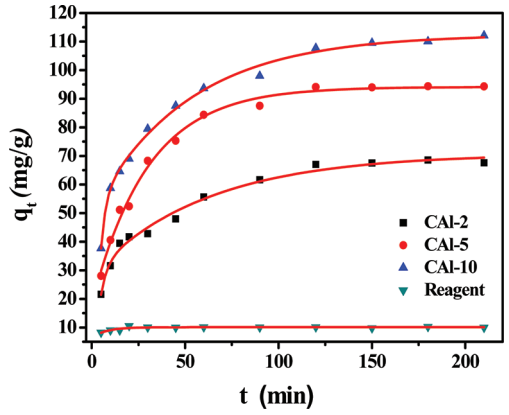

Figure 6. Variation in adsorption capacity with adsorption time for O−II on the CAl-2, CAl-5, CAl-10, and alumina samples (T = 25 °C; adsorbent dose = 200 mg/L; O−II initial concentration = 25 mg/L, and pH 5.0−6.0).

approximately after 120 min. It is noteworthy that the sample CAl-10 achieved the highest capacity of 108 mg/g, which is about ten times more than that of the commercial Al_2O_3 sample. At the pH studied, Orange-II is expected to be adsorbed on the surface of aluminum oxide due to electrostatic attraction between the aluminum oxide shell and sulfonic acid groups of the O−II molecules.[32] The fast O−II uptake is attributed to the combination of several factors, such as high specific surface area, large pore volume, unique rattle-type structure, and high adsorption affinity of the carbon core.[33] Moreover, keeping pH in the range between 5 and 6 facilitated electrostatic interactions because the aluminum oxide surface was positively charged (isoelectric point of $Al_2O_3 \approx 9.0$).[7]

The linear form of the pseudo-second-order kinetic rate model was applied to examine the mechanism of adsorption.[34,35]

$$\frac{t}{q_t} = \frac{1}{k_2 q_e^{\,2}} + \frac{1}{q_e} t \qquad (3)$$

where k_2 (g mg^{-1} min^{-1}) is the rate constant of the second-order adsorption. The linear plot of t/q_t versus t is shown in Figure 7 and the obtained R^2 values are greater than 0.997 for the CAl-2, CAl-5, and CAl-10 samples (Table 2). This indicates

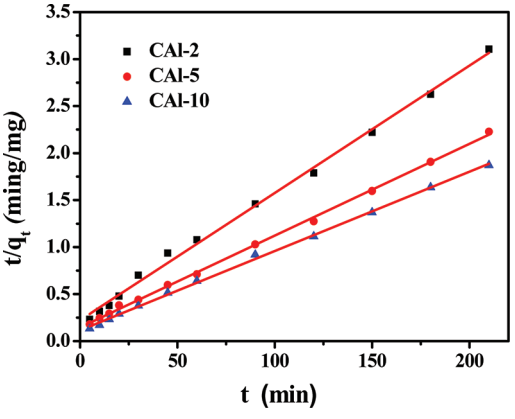

Figure 7. Pseudo-second-order kinetics for adsorption of O−II dye on the CAl-2, CAl-5, and CAl-10 samples (T = 25 °C; adsorbent dose = 200 mg/L; O−II concentration = 25 mg/L, and pH 5.0−6.0).

dx.doi.org/10.1021/am300176k | ACS Appl. Mater. Interfaces 2012, 4, 2174−2179

that the pseudo-second-order model represents well the adsorption kinetics experimental data.

Table 2. Pseudo-second-order Adsorption Kinetic Constants of the Samples studied

			pseudo-second-order model		
sample	C_0 (mg L^{-1})	$q_{e,exp}$ (mg g^{-1})	$q_{e,cal}$ (mg g^{-1})	k_2 ($\times 10^{-4}$ g mg^{-1} min^{-1})	R^2
CAl-2	25	82	74	8.50	0.997
CAl-5	25	118	107	6.44	0.998
CAl-10	25	132	118	4.94	0.999
Al_2O_3	25	10	10	1717	0.999

In addition, the intraparticle diffusion kinetic model based on the theory proposed by Weber and Morris was tested by using the following relation[36]

$$q_t = k_d\sqrt{t} + c \quad (4)$$

where k_d is the rate parameter (mg/g $h^{1/2}$); k_d and c values can be respectively calculated from the slope and intercept of the straight line obtained by plotting q_t vs $t^{1/2}$ (see Figure S1 and Table S1 in the Supporting Information). This figure shows that the linear behavior is observed only in a limited range of time, indicating that this model is not adequate for representing the adsorption kinetics of the systems studied.

Adsorption kinetics data were also measured for O−II dye at different temperatures (25, 35, and 45 °C) in order to evaluate activation energy. Adsorption kinetics data were used to estimate the activation energy (E_a) according to the Arrhenius plot[37]

$$\ln k_2 = \ln A - \frac{E_a}{RT} \quad (5)$$

where E_a is the Arrhenius activation energy (kJ/mol), k_2 is the pseudo-second-order rate constant, A is the Arrhenius factor, R is the gas constant (8.314 J/mol K), and T is the solution temperature. When ln k_2 is plotted versus $1/T$ a straight line with slope $-E_a/R$ is obtained. This estimation gave the value of activation energy (E_a) = 35 kJ/mol, indicating physical adsorption of O−II dye onto the carbon−alumina samples.[38,39]

Adsorption Isotherms. Equilibrium adsorption isotherms for the systems studied are shown in Figure 8. These adsorption isotherms were measured at pH 5−6 and 25 °C.

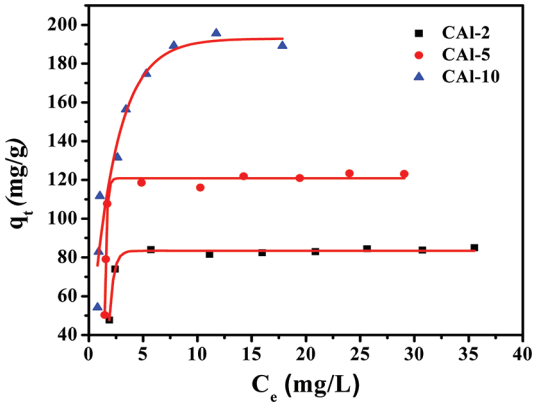

Figure 8. Adsorption isotherms for O−II on the CAl-2, CAl-5, and CAl-10 samples (T = 25 °C; adsorbent dose = 200 mg/L; O−II concentration = 15−50 mg/L, and pH 5.0−6.0).

The Langmuir isotherm equation was used to analyze equilibrium adsorption data; its linear form can be expressed as follows[40,41]

$$\frac{C_e}{q_e} = \frac{1}{q_{max}K_L} + \frac{C_e}{q_{max}} \quad (6)$$

where C_e is the equilibrium concentration of O−II in solution, q_e is the equilibrium amount of O−II on the adsorbent (mg/g), q_{max} is the maximum adsorption capacity of the adsorbent corresponding to the complete monolayer coverage (mg/g), and K_L is the Langmuir adsorption constant, which is related to the Gibbs free energy of adsorption. Note that the original Langmuir equation has been derived for monolayer localized adsorption from an ideal gas phase on an energetically homogeneous surface. This model neglects lateral interactions and assumes adsorption on unoccupied adsorption sites. Although solute adsorption from dilute aqueous solutions can be formally represented by the Langmuir equation, the adsorption mechanism differs from that at the gas/solid interface; in the case of solute adsorption, there is competition between solute and solvent molecules, and the resulting K_L constant depends on the difference of solute and solvent adsorption energies.[42] Figure 9 shows that the Langmuir

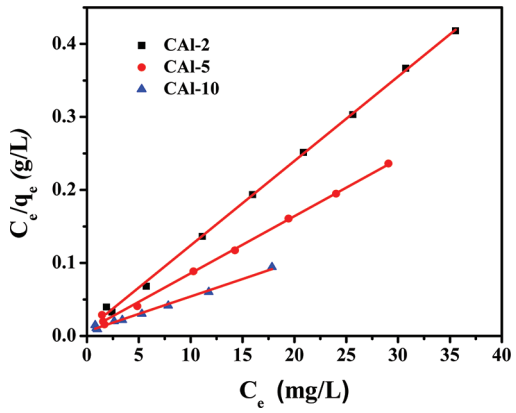

Figure 9. Langmuir linear plots of adsorption isotherms for O−II onto the CAl-2, CAl-5, and CAl-10 samples at 25 °C.

adsorption isotherm fits well with experimental data. The best-fit parameters are listed in Table 3. This implies adsorption of

Table 3. Adsorption Isotherm Parameters of the Samples Studied

	Langmuir adsorption model		
sample	q_{max} (mg/g)	K_L*	R^2
CAl-2	86	4.76×10^5	0.999
CAl-5	131	3.19×10^5	0.998
CAl-10	209	2.67×10^5	0.991

*Although adsorption data are plotted using dye concentration in mg/L, the Langmuir constant values were calculated by expressing the dye concentration in mol/L.

large dye molecules such as O−II dye is represented reasonably well by monolayer localized adsorption model. It is noteworthy that the maximum adsorption capacity of O−II dye on the carbon−alumina spheres prepared in this work is 209 mg/g, which is much higher than that reported for a modified zeolite (3.62 mg/g).[32]

4. CONCLUSIONS

In summary, we have demonstrated the fabrication of rattle-type carbon−alumina particles via a simple and environmentally benign approach involving the one-pot hydrothermal synthesis and calcination. The structurally unique ratle-type particles are composed of porous Al_2O_3 shells and solid carbon cores as well as large free space between the cores and shells. The surface area and porous properties of these composite particles can be significantly improved by simply adjusting the ratio of the glucose and aluminum salt precursors. The adsorption kinetics of Orange-II on the carbon−alumina samples studied follows the pseudosecond-order kinetic model. The equilibrium adsorption data are well represented by Langmuir isotherm equation. These novel rattle-type composite particles with tunable core/shell cavities and high surface area showed good adsorption performance to remove Orange-II dye from water; they are expected to be useful for a variety of applications such as adsorption, catalysis, drug delivery, and especially environmental remediation.

■ ASSOCIATED CONTENT

Supporting Information

One figure and one table showing the adsorption kinetics data and parameters. This material is available free of charge via the Internet at http://pubs.acs.org.

■ AUTHOR INFORMATION

Corresponding Author

*Fax: 86-27-87879468 (J.Y.); 1-330-672-3816 (M.J.). Tel: 86-27-87871029 (J.Y.); 1-330-672-3790 (M.J.). E-mail: jiaguoyu@yahoo.com (J.Y.); jaroniec@kent.edu (M.J.).

Notes

The authors declare no competing financial interest.

■ ACKNOWLEDGMENTS

This work was partially supported by the National Natural Science Foundation of China (51072154, 21177100, and 41173092), Natural Science Foundation of Hubei Province (2010CDA078), National Basic Research Program of China (2009CB939704), and the Self-determined and Innovative Research Funds of WUT (2011-IV-098).

■ REFERENCES

(1) (a) Reis, V.; Guilherme, M. R.; Paulino, A. T.; Muniz, E. C.; Mattoso, L. H. C.; Tambourgi, E. B. *Langmuir* **2009**, *25*, 2473−2478. (b) Ariga, K.; Ishihara, S.; Abe, H.; Li, M.; Hill, J. P. *J. Mater. Chem.* **2012**, *22*, 2369−2377.

(2) (a) Liang, H. P.; Zhang, H. M.; Hu, J. S.; Guo, Y. G.; Wan, L. J.; Bai, C. L. *Angew. Chem., Int. Ed.* **2004**, *43*, 1540−1543. (b) Mandal, S.; Sathish, M.; Saravanan, G.; Datta, K. K. R.; Ji, Q.; Hill, J. P.; Abe, H.; Honma, I.; Ariga, K. *J. Am. Chem. Soc.* **2010**, *132*, 14415−14417. (c) Ambrogio, M. W.; Thomas, C. R.; Zhao, Y. L.; Zink, J. I.; Stoddart, J. F. *Acc. Chem. Res.* **2011**, *44*, 903−913.

(3) Kong, L.; Duan, G.; Zuo, G.; Cai, W.; Cheng, Z. *Mater. Chem. Phys.* **2010**, *123*, 421−426.

(4) (a) Mulvaney, P.; Giersig, M.; Ung, T.; Liz-Marzán, L. M. *Adv. Mater.* **1997**, *9*, 570−575. (b) Ariga, K.; Lvov, Y. M.; Kawakami, K.; Ji, Q.; Hill, J. P. *Adv. Drug Delivery Rev.* **2011**, *63*, 762−771.

(5) (a) Shiomi, T.; Tsunoda, T.; Kawai, A.; Matsuura, S.; Mizukami, F.; Sakaguchi, K. *Small* **2009**, *5*, 67−71. (b) Wu, S. F.; Zhu, Y. Q. *Ind. Eng. Chem. Res.* **2010**, *49*, 2701−2706.

(6) Grzelczak, M.; Correa-Duarte, M. A.; Liz-Marzán, L. M. *Small* **2006**, *2*, 1174−1177.

(7) (a) Cai, W.; Yu, J.; Cheng, B.; Su, B.; Jaroniec, M. *J. Phys. Chem. C* **2009**, *113*, 14739−14746. (b) Ariga, K.; Vinu, A.; Yamauchi, Y.; Ji, Q. M.; Hill, J. P. *Bull. Chem. Soc. Jpn.* **2012**, *85*, 1−32.

(8) (a) Caruso, F.; Spasova, M.; Susha, A.; Giersig, M.; Caruso, R. A. *Chem. Mater.* **2000**, *13*, 109−116. (b) Jones, M. R.; Osberg, K. D.; Macfarlane, R. J.; Langille, M. R.; Mirkin, C. A. *Chem. Rev.* **2011**, *111*, 3736−3827.

(9) Rhodes, K. H.; Davis, S. A.; Caruso, F.; Zhang, B.; Mann, S. *Chem. Mater.* **2000**, *12*, 2832−2834.

(10) Zimmermann, C.; Feldmann, C.; Wanner, M.; Gerthsen, D. *Small* **2007**, *3*, 1347−1349.

(11) Peng, Q.; Dong, Y.; Li, Y. *Angew. Chem., Int. Ed.* **2003**, *42*, 3027−3030.

(12) Yu, J.; Guo, H.; Davis, S. A.; Mann, S. *Adv. Funct. Mater.* **2006**, *16*, 2035−2041.

(13) Yu, J.; Yu, H.; Guo, H.; Li, M.; Mann, S. *Small* **2008**, *4*, 87−91.

(14) Liu, S.; Yu, J.; Jaroniec, M. *J. Am. Chem. Soc.* **2010**, *132*, 11914−11916.

(15) Cai, W.; Yu, J.; Jaroniec, M. *J. Mater. Chem.* **2010**, *20*, 4587−4594.

(16) Wang, J.; Jing, X.; Wang, J.; Ge, L.; Jamil, S.; Zhang, M. *Solid State Sci.* **2010**, *12*, 1934−1940.

(17) (a) Titirici, M. M.; Antonietti, M.; Thomas, A. *Chem. Mater.* **2006**, *18*, 3808−3812. (b) Yu, J.; Yu, X.; Huang, B.; Zhang, X.; Dai, Y. *Cryst. Growth Des.* **2009**, *9*, 1474−1480.

(18) Sun, X.; Liu, J.; Li, Y. *Chem.—Eur. J.* **2006**, *12*, 2039−2047.

(19) Lou, X. W.; Archer, L. A.; Yang, Z. *Adv. Mater.* **2008**, *20*, 3987−4019.

(20) Kamata, K.; Lu, Y.; Xia, Y. *J. Am. Chem. Soc.* **2003**, *125*, 2384−2385.

(21) Zhu, Y.; Kockrick, E.; Ikoma, T.; Hanagata, N.; Kaskel, S. *Chem. Mater.* **2009**, *21*, 2547−2553.

(22) Hah, H. J.; Um, J. I.; Han, S. H.; Koo, S. M. *Chem. Commun.* **2004**, *21*, 1012−1013.

(23) Sing, K. S. W.; Everett, D. H.; Haul, R. A. W.; Moscou, L.; Pierotti, R. A.; Rouquerol, J.; Siemieniewska, T. *Pure Appl. Chem.* **1985**, *57*, 603−619.

(24) Bavykin, D. V.; Parmon, V. N.; Lapkin, A. A.; Walsh, F. C. *J. Mater. Chem.* **2004**, *14*, 3370−3377.

(25) Sevilla, M.; Fuertes, A. B.. *Chem.—Eur. J.* **2009**, *15*, 4195−4203.

(26) Mer, V. K. L. *Ind. Eng. Chem.* **1952**, *44*, 1270−1277.

(27) Deshmukh, A. A.; Mhlanga, S. D.; Coville, N. J. *Mater. Sci. Eng., R* **2010**, *70*, 1−28.

(28) Demir-Cakan, R.; Baccile, N.; Antonietti, M.; Titirici, M. M. *Chem. Mater.* **2009**, *21*, 484−490.

(29) Tu, C. M.; Davis, H.; Hottel, H. C. *Ind. Eng. Chem.* **1934**, *26*, 749−757.

(30) Yu, J.; Yu, X. *Environ. Sci. Technol.* **2008**, *42*, 4902−4907.

(31) Zhou, J.; Yang, S.; Yu, J. *Colloids Surf., A* **2011**, *379*, 102−108.

(32) Jin, X.; Jiang, M.; Shan, X.; Pei, Z.; Chen, Z. *J. Colloid Interface Sci.* **2008**, *328*, 243−247.

(33) Guo, L.; Zhang, L.; Zhang, J.; Zhou, J.; He, Q.; Zeng, S.; Cui, X.; Shi, J. *Chem. Commun.* **2009**, *40*, 6071−6073.

(34) Tan, I. A. W.; Ahmad, A. L.; Hameed, B. H. *J. Hazard Mater.* **2009**, *164*, 473−482.

(35) Ho, Y. S.; McKay, G. *Chem. Eng. J.* **1998**, *70*, 115−124.

(36) Weber, W. J.; Morris, J. C. *Pergamon* **1962**, *2*, 231−262.

(37) Zhou, J.; Cheng, Y.; Yu, J.; Liu, G. *J. Mater. Chem.* **2011**, *21*, 19353−19361.

(38) Nollet, H.; Roels, M.; Lutgen, P.; Van der Meeren, P.; Verstraete, W. *Chemosphere* **2003**, *53*, 655−665.

(39) Fan, J.; Cai, W.; Yu, J. *Chem. Asian J.* **2011**, *6*, 2481−2490.

(40) (a) Hameed, B. H.; Ahmad, A. A.; Aziz, N. *Chem. Eng. J.* **2007**, *133*, 195−203. (b) Zhou, J.; Yang, S.; Yu, J.; Shu, Z. *J. Hazard Mater.* **2011**, *192*, 1114−1121.

(41) Langmuir, I. *J. Am. Chem. Soc.* **1918**, *40*, 1361−1403.

(42) Jaroniec, M.; Madey, R. *Physical Adsorption on Heterogeneous Solids*; Elsevier: Amsterdam, 1988.